Journal of Colloid and Interface Science 648 (2023) 1015–1024

Contents lists available at ScienceDirect

Journal of Colloid And Interface Science

journal homepage: www.elsevier.com/locate/jcis

Application of community data to surface complexation modeling framework development: Iron oxide protolysis

Sol-Chan Han [a], Elliot Chang [a], Susanne Zechel [b], Frank Bok [b], Mavrik Zavarin [a,*]

[a] Seaborg Institute, Lawrence Livermore National Laboratory, 7000 East Avenue, Livermore, CA 94550, United States
[b] Institute of Resource Ecology, Actinide Thermodynamics Department (FWOA), Helmholtz-Zentrum Dresden-Rossendorf, Bautzner Landstraße 400, 01328 Dresden, Germany

GRAPHICAL ABSTRACT

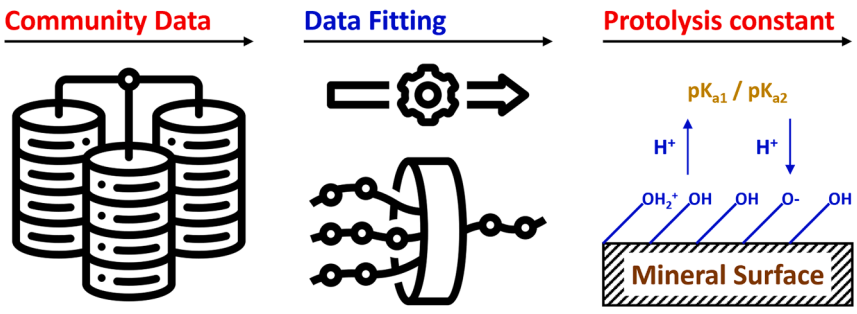

ARTICLE INFO

Keywords:
Sorption
Protolysis
Iron Oxide
Radionuclide
Surface Complexation
Potentiometric Titration

ABSTRACT

This study presents a comprehensive community data-driven surface complexation modeling framework for simulating potentiometric titration of mineral surfaces. Compiled community data for ferrihydrite, goethite, hematite, and magnetite are fit to produce representative protolysis constants that can reproduce potentiometric titration data collected from multiple literature sources. Using this framework, the impact of surface complexation model type and surface site density (SSD) on the fit quality and protolysis constants can be readily evaluated. For example, the non-electrostatic model yielded a poor data fit compared to diffuse double layer model and constant capacitance models due to the absence of known surface charge effects. Regardless of the choice of iron oxide mineral, pK$_{a1}$ decreased with increasing SSD while the opposite tendency was observed for pK$_{a2}$. This newly developed framework demonstrates a method to reconcile community data-wide potentiometric titration data using Findable, Accessible, Interoperable, Reusable data principles to produce mineral protolysis constants that improve robustness of surface complexation models for applications in metal sorption and reactive transport modeling. The framework is readily expandable (as community data increase) and extensible (as the number of minerals increase). The framework provides a path forward for developing self-consistent, comprehensive, and updateable surface complexation databases for surface complexation and reactive transport modeling.

* Corresponding author.
E-mail address: zavarin1@llnl.gov (M. Zavarin).

https://doi.org/10.1016/j.jcis.2023.06.054
Received 13 March 2023; Received in revised form 16 May 2023; Accepted 9 June 2023
Available online 10 June 2023

1. Introduction

Among the various chemical interactions at the mineral–water interface, adsorption is considered one of the key mechanisms that controls the transport of chemical species in the environment. Historically, linear distribution coefficients (K_d) have been used to represent this retardation process [1]. Although the K_d approach is very simple to implement, using K_d values in reactive transport models poses some limitations. For instance, the approach cannot account for changes in geochemical conditions (e.g. pH and solution ionic strength) [2], and maximum adsorption capacity [3], ultimately compromising the flexibility and applicability of K_d-based approaches.

Over several decades, numerous surface complexation models (SCMs) have been developed to quantify the adsorption process occurring at the mineral–water interface and address the limitations of the K_d approach. In contrast to the K_d approach, SCMs are based on a chemical equilibrium approach and adopt mass action laws (equations) to describe equilibrium between aqueous species and adsorbed species [4–7]. Therefore, SCMs can address spatial and temporal variations in geochemical conditions and their impact on retardation.

The functional form of a SCM can vary significantly. For example, the non-electrostatic model (NEM) is the simplest form of SCM as it neglects the impact of an electric double layer (and associated surface potential) on surface reaction equilibria. Nevertheless, it has been shown to effectively predict field scale transport behavior in some cases [8]. The diffuse double layer model (DDLM) includes a simple relationship between surface charge and surface potential

$$\sigma = 0.1174 \times I^{1/2} \times sinh(19.46 \times Z \times \psi) \quad (1)$$

at 25 °C where σ is the surface charge (C m^{-2}), Z is the charge of a symmetric electrolyte, I is the ionic strength, and Ψ is the surface potential (volts) with all surface reactions occurring at a single (inner sphere) plane. The difference between an apparent and intrinsic surface complexation constant can be calculated by

$$K_{app} = K_{int} \times exp\left(\frac{-\Delta Z F \psi}{RT}\right) \quad (2)$$

where K_{app} and K_{int} are the apparent and intrinsic surface complexation constant, respectively, ΔZ is the change in surface charge, F is the Faraday constant (96490C mol^{-1}), R is the gas constant (8.314 J mol^{-1} K^{-1}), and T is the temperature (K) [9]. Due to its relative simplicity, it has often been employed in the development of comprehensive SCM databases (e.g. [10,11]) and reactive transport codes (e.g. PHREEQC [12], CrunchFlow [13]). More complex functional forms of SCMs also exist, including the triple-layer SCM (TLM) [14] that accounts for both inner sphere and outer-sphere sorption phenomena and the CD-MUSIC model [15] that accounts for multiple surface sites and strict stoichiometry relationships. Even more complex representations of mineral–water interface reactions such as those that account for charge "spillover" effects on clay surfaces [16] are being developed in the case of heterogeneous surface characteristics.

Since protolysis reactions on mineral surfaces are fundamental to the description of adsorption [17], parameters describing surface protolysis reactions (i.e. reaction constants) are needed [18] regardless of the SCM type. A typical example of surface functional groups occurring on oxide or clay minerals are reactive hydroxyl groups. These functional groups participate in protolysis reactions (i.e., protonation and deprotonation reactions), leading to charge build-up on the surface of solid adsorbents [19]. In SCMs, the following two reactions and associated reaction constants are widely used to describe the protolysis of surface hydroxyl groups [10,20]:

$$\gg SOH_2^+ \rightleftharpoons \gg SOH^0 + H^+$$
$$K_{a1}^{int} = \frac{(\gg SOH^0)\{H^+\}}{(\gg SOH_2^+)} exp\left(\frac{-F\Psi}{RT}\right),\ pK_{a1} = -logK_{a1} \quad (3)$$

Table 1
Diffuse double layer surface complexation model protolysis constants and site densities for ferrihydrite reported in the literature. Data from RES^{3}T database [35,36].

	1st protolysis constant (pK_{a1})	2nd protolysis constant (pK_{a2})	Site density (sites·nm^{-2})
1[a]	6.09	7.38	2.2583
2[b]	6.51	9.13	0.0203
3[c]	7	9.2	7.0903
4[d]	7.01	7.86	0.7300
5[e]	7.29	8.93	2.2553
6[f]	7.5	10.2	9.9966

[a] [34]; [b][33]; [c][29]; [d][30]; [e][31]; [f][32].

$$\gg SOH^0 \rightleftharpoons \gg SO^- + H^+$$
$$K_{a2}^{int} = \frac{(\gg SO^-)\{H^+\}}{(\gg SOH^0)} exp\left(\frac{-F\Psi}{RT}\right),\ pK_{a2} = -logK_{a2} \quad (4)$$

where () represents concentrations, { } represents activities, and ΔZ = -1. The equilibrium constants K_{a1}^{int} and K_{a2}^{int} are the first and the second intrinsic protolysis constants, respectively. The increased formation of »SOH_2^+ compared to »SO^- at low pH conditions induces a net positive surface charge while at high pH, the surface becomes negatively charged due to the increased formation of »SO^- in comparison to »SOH_2^+ [20]. SCMs, thus, can account for the impact of protolysis reactions (and surface charge development) on the adsorption of anions or cations to the solid adsorbent under variable pH conditions.

From the perspective of nuclear waste disposal and repository performance assessment, the sorption of radionuclides to iron oxide minerals is of great importance for several reasons. Iron oxide minerals are commonly found in bedrock, soils, and sediments that host underground nuclear waste repositories. Furthermore, the corrosion of engineered barriers in radioactive waste repositories will lead to the formation of iron oxides [21]. Iron oxide minerals, thus, may provide a significant source of radionuclide sorption and retardation both in the near- and far-field of a nuclear waste repository. More generally, as iron oxides exert a high affinity for pollutants such as heavy metals and organic xenobiotics, they have taken on important roles in not only nuclear waste disposal but also in general environmental remediation technologies. Iron oxide minerals also have an excellent potential to efficiently sorb oxyanions [22], while most natural clay minerals exhibit weak to intermediate anion adsorption capacities [23]. These facts have led to significant research interest regarding the sorption properties of iron oxides and, in turn, an interest in understanding the fundamental characteristics of iron oxides [24]. This research has included experimental (e.g., potentiometric titrations: [25–27]) and theoretical (e.g., [17,28]) studies of the protolysis characteristics of iron oxide surfaces.

Although considerable effort has been made to understand protolysis characteristics of iron oxides and to develop reliable SCMs for iron oxide adsorption, a present-day challenge still exists in determining which SCMs and associated reaction parameters are most appropriate for downstream reactive transport models. In various studies [29–34], different surface protolysis constants have been reported even in the case when the same type of SCM and iron oxide mineral were under investigation (see Table 1). This fact leads to ambiguity in the selection of 'representative' protolysis constants and uncertainty in the further development of self-consistent surface complexation databases. In other words, there now exists an impasse in the integration of the experimental data scattered in different studies into comprehensive SCM frameworks that reconcile the full community-wide data.

In light of this challenge, this study aims at integrating and modeling digitized and compiled potentiometric titration data, reported following the Findable, Accessible, Interoperable, Reusable (FAIR) data principles [37], through the Lawrence Livermore National Laboratory Surface Complexation/Ion Exchange (L-SCIE) database [38]. The surface

Table 2
Description of iron oxide potentiometric titration data used in this study.[a.]

Iron oxide minerals	Data count	No. of datasets	No. of references	pH range
Ferrihydrite	1,119	40	12	2.7 – 11.7
Goethite	1,982	79	23	3.0 – 11.0
Hematite	1,702	61	16	2.7 – 11.1
Magnetite	301	14	8	2.3 – 12.0

[a] Potentiometric titration data included in the L-SCIE database and evaluated here include: 1) ferrihydrite: [25–27,39–47], 2) goethite: [18,25,26,48–67], 3) hematite: [59,67–81], and 4) magnetite: [51,82–88].

complexation modeling focuses on fitting compiled community data for each individual iron oxide mineral (i.e., ferrihydrite, goethite, hematite, and magnetite) to produce representative protolysis constants that account for all potentiometric titration data collected from multiple literature sources. In addition, the effect of surface site density (SSD) on protolysis constants is analyzed by means of sensitivity analysis, as variation of SSD used in proton adsorption modeling is known to be a major cause for deviations in reported protolysis constants [24]. It is expected that the modeling framework described herein and results obtained from the present study can reconcile large amounts of potentiometric titration data. By providing the most appropriate protolysis constants (and associated parameter uncertainties), this study provides improved constraints to be utilized in downstream SCM development, such as in the modeling of radionuclide sorption onto iron oxide minerals in nuclear waste repository performance assessment. The framework also provides a path forward for developing self-consistent, comprehensive, and updateable FAIR surface complexation databases for reactive transport modeling more broadly.

2. Surface complexation modeling framework

As part of this effort, a surface complexation modeling framework was developed. This framework consists of two major components: (1) a community sorption database and workflow (i.e., L-SCIE [38]) that provides FAIR community potentiometric titration data and (2) a potentiometric titration modeling workflow that automates fitting of protolysis constants for selected SCM type (e.g. NEM, DDLM, etc.) to community potentiometric titration data.

2.1. The L-SCIE database and workflow

The L-SCIE database and workflow was developed with the aim of compiling raw community sorption data which can, in turn, be used in downstream SCM database development. The L-SCIE database contains not only raw sorption data, including potentiometric titration data digitized from the literature, but also relevant metadata (e.g., experimental conditions), and is stored as a Microsoft Access format [38]. In order to use the compiled raw sorption data, the raw data are processed through a workflow of unit conversions which include error propagation. Once data "unification" has been completed, the community data can be filtered based on the type of mineral, adsorbate, etc. for downstream processing (e.g., surface complexation modeling). In this study, potentiometric titration data for four iron oxide minerals (i.e., ferrihydrite, goethite, hematite, and magnetite) were evaluated. It should be noted that the data used in this study (Table 2) was extracted from the L-SCIE database and may not reflect all available data in the literature. Nevertheless, since our SCM framework is based on the FAIR data principle, one can easily refit the protolysis constants as new data become available.

2.2. The potentiometric titration data workflow

A workflow was developed to model the potentiometric titration data contained in the L-SCIE database. The workflow was coded in Python and coupled to PHREEQC [12] for surface complexation modeling and PEST [89] for data fitting and parameter (protolysis constants) estimation. The details of the workflow are shown in Fig. 1. First, the community data prepared from the L-SCIE database is imported into Python. Since a single reference may include multiple datasets depending on experimental conditions (e.g., ionic strength), all data are binned by dataset. PHREEQC is first called to perform a charge balance on each datapoint by adjusting the concentration of background electrolyte concentration (e.g. Na^+, Cl^-) and to enhance the stability of follow-on geochemical fitting routines. PHREEQC/PEST input files for each dataset are then generated, PHREEQC/PEST fitting is performed for each dataset separately, and simulation results are exported into a summary file. Finally, weighted arithmetic mean pK_{a1} and pK_{a2} values of all datasets are calculated to produce 'representative' average protolysis constants (see the relevant description in Section 2.3).

2.3. Calculation of weighted arithmetic mean protolysis constants

Once the PHREEQC/PEST fitting is performed for each dataset, the PEST code produces two protolysis constants (pK_{a1} and pK_{a2}) and associated 95% confidence intervals ($\pm 2\sigma$) for each dataset. In this study, the weighted arithmetic mean was used to calculate 'representative' average pK_a values for the entire community dataset. Weighted average (x_{wav}) is the best estimation for the true x value when there are N measurements of$x$ with corresponding uncertainties (i.e., $x_1 \pm \sigma_1$, …, $x_N \pm \sigma_N$), and can be calculated by the following Eqs. (5) and (6) [90,91]:

$$x_{wav} = \frac{\sum w_i x_i}{\sum w_i} \tag{5}$$

$$w_i = \frac{1}{\sigma_i^2} \tag{6}$$

where x_i denotes i^{th} measurement of x and w_i represents the corresponding weight which is the reciprocal square of uncertainty of i^{th} measurement (σ_i). Finally, uncertainty in the weighted average can be calculated by Eq. (7) [90]:

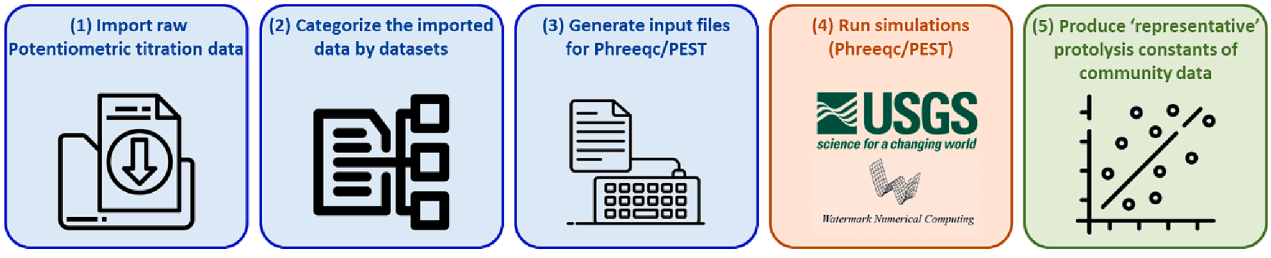

Fig. 1. Surface complexation modeling workflow for potentiometric titration data.

Table 3
Surface site densities of ferrihydrite, goethite, hematite, and magnetite.

Iron oxide mineral	Crystallographically-Derived SSD (sites·nm^{-2})	Iron oxide mineral	Crystallographically-Derived SSD (sites·nm^{-2})
Ferrihydrite	6.53	Hematite	5.83
Goethite	6.60	Magnetite	4.56

$$\sigma_{wav} = \sqrt{\frac{\sum w_i (x_i - x_{wav})^2}{\frac{(N'-1)\sum w_i}{N'}}} \quad (7)$$

where N' denotes the number of non-zero weights. In our case, total number of measurements, N, is equal to total number of datasets, x_i corresponds to pK_{a1} or pK_{a2} from the i^{th} dataset and σ_i is the uncertainty of pK_{a1} or pK_{a2} from the i^{th} dataset.

2.4. Sensitivity analysis of surface site density

In this study, surface site densities (SSD) of iron oxides were obtained using a crystallographic approach [92,93]. Crystallographic literature data for ferrihydrite, goethite, hematite and magnetite were collected and evaluated, considering only measurements at T = 25 °C and atmospheric pressure [94–97]. Ferrihydrite surface planes were predicted by Bravais-Friedel-Donnay-Harker (BFDH) morphology calculations [98] using the Mercury software code [99] whereas for goethite the most common faces mentioned in the literature where used [24,100,101]. According to literature, the minerals hematite and magnetite mostly occur in certain crystal habits [100,101]. The faces of these crystal forms were used for the SSD estimation.

Natural iron(hydr-)oxides are not expected to form perfectly crystallized, single habits, but rather multiple intergrown crystallites. Known minor crystal faces, which occur only occasionally and with small areal ratios, were omitted. Using crystallographic data, the positions of interfacial oxygen atoms were calculated for each surface plane on the most stable termination with octahedral iron-oxygen coordination. There, surface unit cells delimited by four crystallographically identical oxygen atoms were defined and the number of all surface oxygen atoms within the unit cell was determined. As surface oxygen positions are expected to be identical to the positions of > Fe-OH binding groups at the iron(hydr-)oxide surface, the SSDs were calculated for each plane using the outermost oxygen atoms. A distinction was made between singly (≡FeOH) and doubly ($\equiv Fe_2O$) coordinated groups. For an overall SSD value, the weighted mean using the relative area ratios was determined (see Table 3).

The crystallographically-derived SSDs for singly coordinated groups on ferrihydrite, goethite, hematite, and magnetite are 6.53, 6.60, 5.83, and 4.56 sites·nm^{-2}, respectively. These values were used in the estimation of protolysis constants. However, natural minerals likely include irregularities that may cause variation in SSD values. For this reason, sensitivity analysis of SSD was also conducted to examine the effect of SSD on pK_a estimation. The SSDs applied in the sensitivity analysis ranged from 3 to 10 sites·nm^{-2} (i.e., 3, 5, 7, and 10 sites·nm^{-2}). An SSD of 2.31 sites·nm^{-2}, suggested by Dzombak and Morel [10] for hydrous ferric hydroxide, has previously been recommended for use in estimating binding constants on many types of minerals [6]. For this reason, many studies have employed this SSD [102]. In our sensitivity analysis, 2.31 sites·nm^{-2} was also included considering the fact that the value has been conventionally used in a number of surface complexation modeling efforts.

3. Results and discussion

3.1. Diffuse double layer model protolysis constants of ferrihydrite, goethite, hematite, and magnetite

The iron oxide pK_a values were estimated by fitting the community potentiometric titration data using the SCM framework described above. The DDLM was initially adopted to describe the electrical double layer, and SSDs obtained from the aforementioned crystallographic approach were used. The resulting iron oxide pK_a values (Eqs. (3) and (4)) are summarized in Table 4. In the table, average pK_a values reported in the RES^{3}T database [35,36] are also included for comparison. These values are simply an average of all reported values without any evaluation of

Table 4
Diffuse double layer model protolysis constants for iron oxides as a function of surface site density.

Iron oxides	SSD (sites·nm^{-2})	pK_{a1} ††	pK_{a2} ††	R value	RES^{3}T pK_{a1}	RES^{3}T pK_{a2}
Ferrihydrite	2.31	6.7 ± 0.4	8.7 ± 0.6	0.916	7.2 ± 0.2	9.0 ± 0.2
	3	6.5 ± 0.4	8.7 ± 0.6	0.916		
	5	6.2 ± 0.4	8.9 ± 0.6	0.915		
	6.53†	**6.1 ± 0.4**	**9.0 ± 0.6**	**0.915**		
	7	6.1 ± 0.4	9.0 ± 0.6	0.915		
	10	5.9 ± 0.4	9.2 ± 0.6	0.916		
Goethite	2.31	6.9 ± 0.8	9.1 ± 0.7	0.880	7.1 ± 0.5	9.9 ± 0.8
	3	6.7 ± 0.7	9.2 ± 0.7	0.877		
	5	6.4 ± 0.7	9.4 ± 0.7	0.868		
	6.60†	**6.2 ± 0.7**	**9.5 ± 0.6**	**0.867**		
	7	6.2 ± 0.7	9.6 ± 0.6	0.867		
	10	6.0 ± 0.7	9.7 ± 0.6	0.868		
Hematite	2.31	7.6 ± 0.7	9.2 ± 0.8	0.875	6.8 ± 0.6	9.0 ± 0.9
	3	7.3 ± 0.7	9.3 ± 0.9	0.877		
	5	6.9 ± 0.8	9.4 ± 0.8	0.874		
	5.83†	**6.8 ± 0.8**	**9.4 ± 0.8**	**0.872**		
	7	6.7 ± 0.8	9.5 ± 0.8	0.873		
	10	6.5 ± 0.8	9.6 ± 0.8	0.872		
Magnetite	2.31	6.2 ± 0.2	7.3 ± 0.2	0.922	5.1 ± 0.8	8.3 ± 1.2
	3	6.1 ± 0.2	7.5 ± 0.4	0.923		
	4.56†	**5.9 ± 0.2**	**7.4 ± 0.6**	**0.935**		
	5	5.8 ± 0.2	7.5 ± 0.6	0.934		
	7	5.7 ± 0.3	7.6 ± 0.7	0.940		
	10	5.5 ± 0.3	7.6 ± 0.7	0.944		

† Crystallographically-derived surface site density (used as reference case).
†† Reported uncertainties are mean weighted ± σ of the fitted pK_a values (Eq. (7)). Note that the RES^{3}T pK_a uncertainties are simply the standard deviations of the values reported in the database.

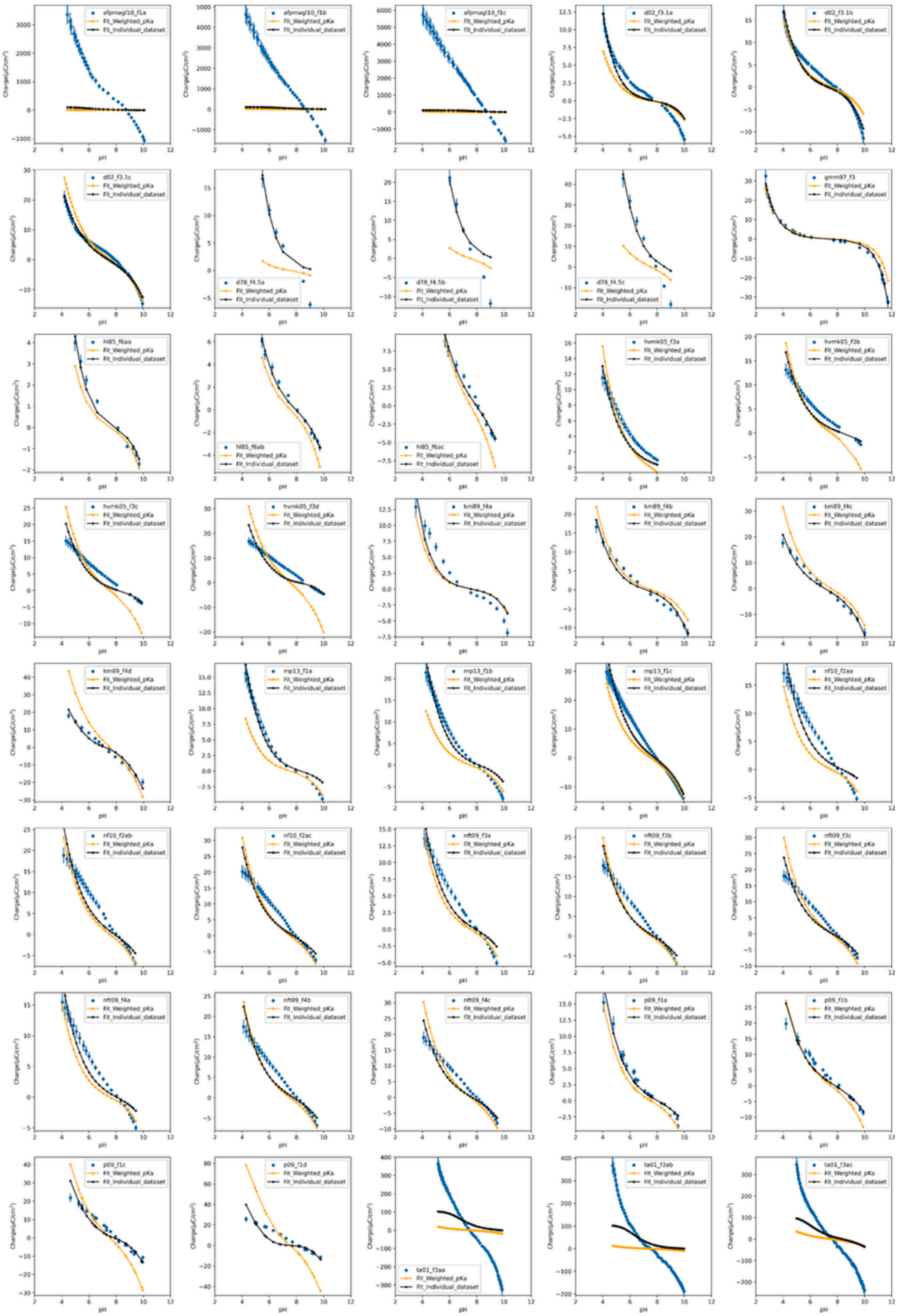

Fig. 2. Potentiometric titration data of ferrihydrite (blue), modeling data using weighted mean DDLM pK_a values (orange), and DDLM fits obtained for individual datasets (black). All models used the crystallographically-derived surface site density (Table 4). Error bars represent estimated data uncertainties at one standard deviation.

the source (i.e., data redundancy, provenance, etc.).

Sverjensky [28] theoretically calculated the protolysis constants of minerals based on a TLM. The calculated protolysis constants were found to increase in the order: magnetite < ferrihydrite < goethite < hematite. As shown in Table 4, protolysis constants calculated in the present study, using crytallographically-derived SSD values for each mineral, have a similar tendency. It should be noted that pK_{a2} of hematite, calculated in our model, is slightly lower than that of goethite, and differences in pK_a values of ferrihydrite, goethite, and hematite are not all statistically significant. However, pK_a values of magnetite are clearly lower than the three other iron oxide minerals.

It is plausible that the order of protolysis constants of iron oxides is highly correlated to their respective thermodynamic stabilities. In other words, the pK_a values of iron oxides increase with increasing thermodynamic stability of the solid phase: ferrihydrite < goethite ≤ hematite [24,103–109]. As stated above, pK_{a2} of hematite is slightly lower than goethite while pK_{a1} of hematite is higher than goethite. Thus, the order of protolysis constants of goethite and hematite is ambiguous. Interestingly, the thermodynamic stabilities of goethite and hematite are also similar [24,104], and relative stability of goethite to hematite (with water) is uncertain as well [110,111]. The difference in iron oxidation state of magnetite and the three other oxides, i.e., Fe(II, III) for magnetite and Fe(III) for ferrihydrite, goethite, and hematite, seems to be a major reason for magnetite having distinct protolysis constants.

Ferrihydrite potentiometric titration data, model fits using weighted mean pK_a values, and fits to individual datasets are shown in Fig. 2. In general, the fits to individual datasets outperform the fits using weighted mean pK_a values. This suggests that sample characteristics likely vary among the various datasets and yield different surface charging properties. Nevertheless, with the exception of a few datasets, a single set of weighted mean pK_a values can represent the community potentiometric titration data reasonably well.

In the case of some datasets, the fitted model did not reproduce the experimental data. The poor fit to the data is, in most cases, indicative of erroneous reporting of potentiometric titration data. For example, Antelo et al. [46] reported potentiometric titration data in Fig. 1 of their publication (afpmagl10) that reached nearly 6000 $\mu C \cdot cm^{-2}$ at low pH and 0.5 M KNO_3. This is more than two orders of magnitude higher than most reported values and likely represents a typographical error in the publication. Importantly, given that our mean value is weighted by the associated parameter uncertainty (see Eq. (7)), the erroneous data (i.e., [46]) do not significantly impact the weighted mean pK_a values for ferrihydrite. If we simply remove those datasets (i.e., afpmagl10_f1a, afpmagl10_f1b, and afpmagl10_f1c) from our analysis, the resulting pK_{a1} and pK_{a2} for ferrihydrite is 6.1 and 9.0, respectively, which is identical to the values reported in Table 4. Similarly, Trivedi and Axe [26] reported unusually high surface charges on ferrihydrite (up to 400 $\mu C \cdot cm^{-2}$). However, the authors acknowledged that the high surface charging is likely the result of the unusually low reported BET surface area (36.6 $m^2 \cdot g^{-1}$) compared to ~ 600 $m^2 \cdot g^{-1}$ that is commonly reported for this amorphous mineral [10]. The modeling results for all iron oxides and SCM types are reported in the Supplementary Material.

3.2. Effect of type of electrical double layer

In order to build a self-consistent SCM reaction database, protolysis constants should be estimated using a consistent SCM type (e.g., NEM, DDLM, or constant capacitance model (CCM)) which, in turn, is identical to that used for downstream sorption modeling. In the present study, we examined how the SCM type affects the protolysis constants and evaluated how well each SCM type reproduces the potentiometric titration data. The modeling was conducted for four iron oxides (i.e., ferrihydrite, goethite, hematite, and magnetite) and three types of SCM: NEM, DDLM, and CCM.

Surface complexation modeling results for ferrihydrite using the NEM and CCM are illustrated in Figures S1 and S3, respectively. In contrast to DDLM (Fig. 2), the NEM rarely reproduced experimentally obtained potentiometric titration data of ferrihydrite. The most remarkable feature observed in the NEM fits was that the modeled surface charge rapidly increased or decreased at low and high pH (e.g., Fig. 3). Since the NEM neglects the impact of an electric double layer and associated surface potential, the model cannot address repulsion and/or attraction effects between proton and surface induced by surface charge build-up. Therefore, the shape of the NEM fitting is mainly affected by the activity of proton in solution. As a result, the NEM has relatively steep slopes in comparison to the DDLM (e.g., Fig. 3), and pK_{a1} of the NEM is lower than that of the DDLM, while pK_{a2} of the NEM is higher than that of the DDLM (Table 5). The CCM is effective at reproducing most of the potentiometric titration data. However, it was relatively less effective for magnetite potentiometric titration data. In addition, as is

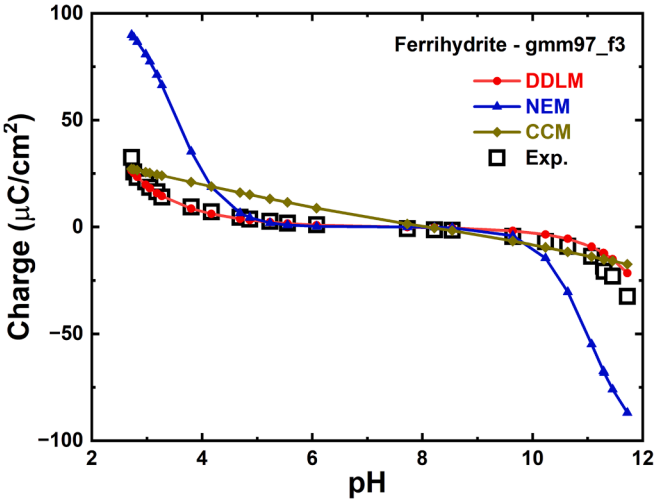

Fig. 3. Comparison of modeling results using the NEM, CCM, and DDLM for a single ferrihydrite dataset. The gmm97_f3 refers to a potentiometric titration dataset reported in [41] and performed on 10 g/L ferrihydrite in a 0.001 M NaCl solution.

Table 5
Estimated protolysis constants of iron oxide minerals with different surface complexation models using crystallographically estimated surface site densities (Table 3).

Iron oxides	SCM type	pK_{a1}	pK_{a2}	$(pK_{a1} + pK_{a2})/2$	Capacitance
Ferrihydrite	NEM	3.51 ± 0.65	11.03 ± 0.57	7.27 ± 0.43	–
	DDLM	6.09 ± 0.40	9.00 ± 0.56	7.55 ± 0.34	–
	CCM	6.41 ± 0.38	9.78 ± 0.39	8.10 ± 0.27	1.11 ± 0.52
Goethite	NEM	5.06 ± 1.08	9.96 ± 1.10	7.51 ± 0.77	–
	DDLM	6.23 ± 0.69	9.54 ± 0.63	7.89 ± 0.47	–
	CCM	6.93 ± 0.37	10.90 ± 0.33	8.92 ± 0.25	0.90 ± 0.18
Hematite	NEM	3.99 ± 0.61	10.83 ± 0.61	7.41 ± 0.43	–
	DDLM	6.84 ± 0.75	9.42 ± 0.79	8.13 ± 0.54	–
	CCM	7.25 ± 0.39	10.94 ± 0.44	9.10 ± 0.29	1.07 ± 0.22
Magnetite	NEM	4.17 ± 0.70	8.73 ± 1.46	6.45 ± 0.81	–
	DDLM	5.85 ± 0.22	7.44 ± 0.60	6.65 ± 0.32	–
	CCM	6.06 ± 0.37	6.07 ± 0.36	6.07 ± 0.26	2.08 ± 1.46

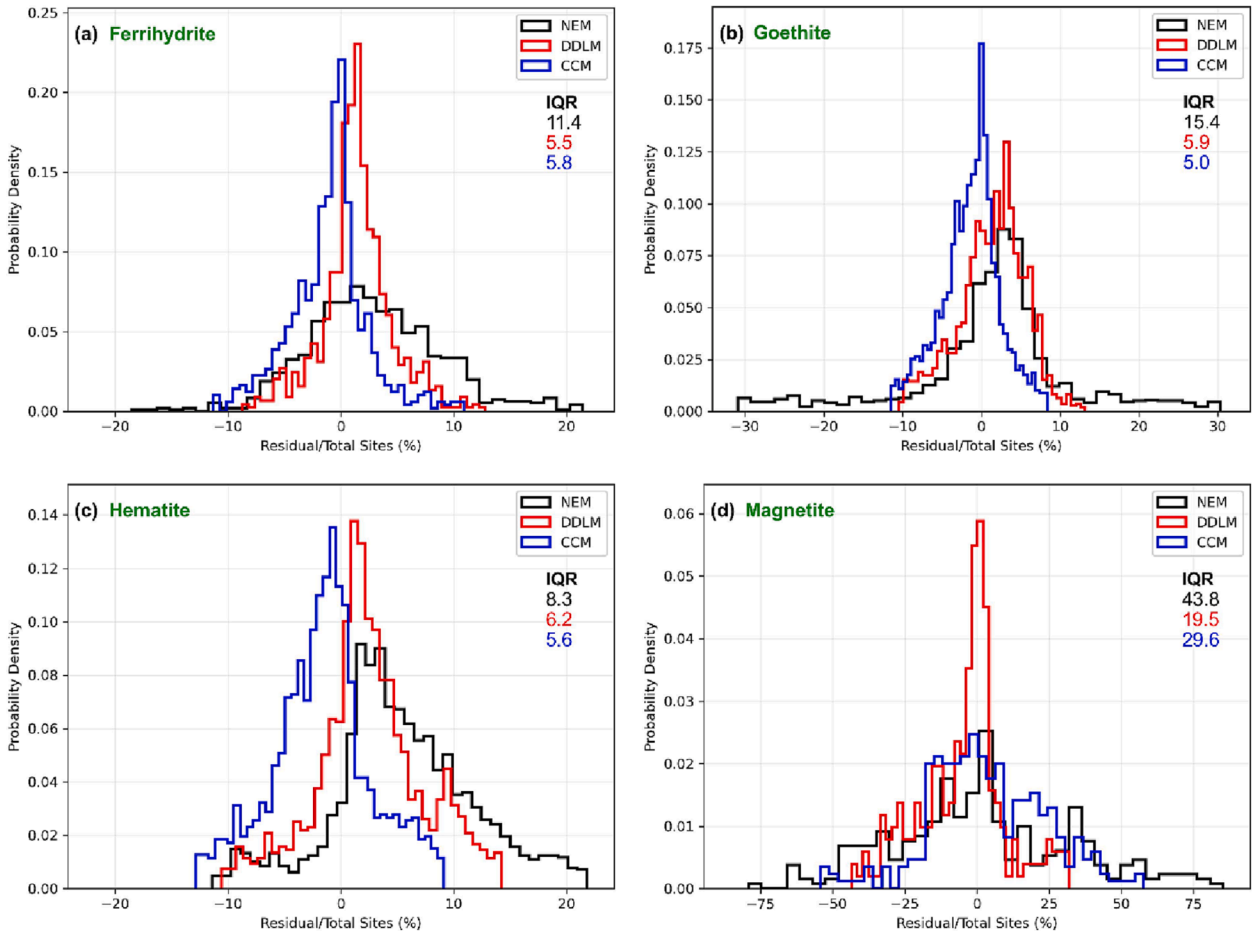

Fig. 4. Normalized histograms as a percent difference between the experimental and modeled surface charge for NEM, DDLM, and CCM models of (a) ferrihydrite, (b) goethite, (c) hematite, and (d) magnetite. The bin size of each histogram is equivalent to one tenth of IQR.

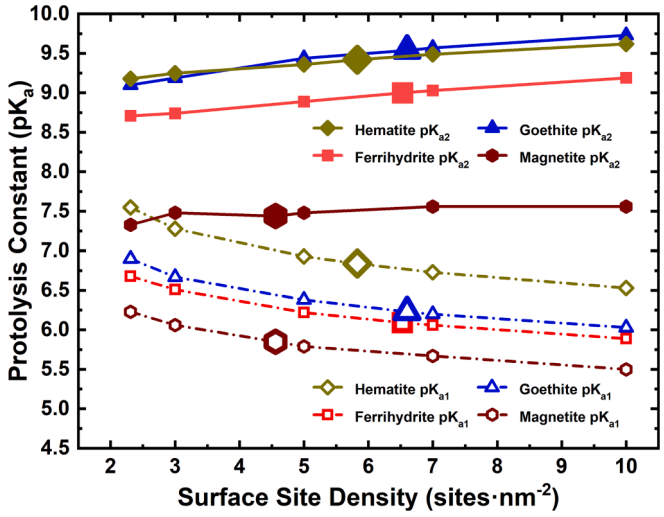

Fig. 5. Diffuse double layer model protolysis constants for iron oxides as a function of surface site density. Large symbols represent the protolysis constants obtained with crystallographically-derived surface site density.

well known, the CCM performs better in high ionic strength solutions and tends to fail at low ionic strength (e.g., Fig. 3) [18,112]. Theoretically, the CCM is valid for low interfacial potentials and, as a result, is most applicable to high ionic strength solutions (i.e., greater than 0.01 M) [18].

The type of SCM also significantly affects the quality of fit. Fig. 4 illustrates the fit quality for each SCM type and mineral phase in the form of normalized histograms as a percent difference between the experimental and modeled surface charge (e.g. a 10% value on the x-axis represents a 10% difference between experimental and modeled surface charge). The interquartile ranges (IQRs) of weighted residual data obtained from the models using each SCM type are also reported. The histograms exclude outliers where the data points fall below Q_1 (first quartile of the data) – 1.5 × IQR or above Q_3 (third quartile of the data) + 1.5 × IQR.

As shown in Fig. 4, the IQR of the NEM is always greater than the IQR of the DDLM and CCM. This implies that the fit quality of DDLM and CCM is overall better than that of the NEM. Although the NEM can effectively be used to predict the adsorption behavior of various adsorbates (e.g., [8]), it fails to accurately reproduce mineral surface protolysis. In the case of adsorbate sorption systems, the number of surface sites is expected to be significantly higher than the amount of adsorbate. Therefore, the effect of charge build-up due to adsorbate sorption might be negligible. In the surface protolysis case, however, a high proportion of surface sites is protonated or deprotonated, making the charge build-up non-negligible.

3.3. *Effect of surface site density on protolysis constants*

As summarized in Table 4 and Fig. 5, the value chosen for SSD significantly affects the modeled pK_a values for iron oxides. The most remarkable observation was that pK_{a1} decreased with increasing SSD, while pK_{a2} increased with increasing SSD. This systematic tendency was

consistent regardless of the type of iron oxide mineral and is in good agreement with other studies [18,74,79].

The quality of DDLM fit (R value) derived based on each SSD value is given in Table 4. The R value, equivalent to a weighted Pearson correlation coefficient [38], was calculated excluding outliers discussed in Section 3.2. As evident in Table 4, no clear correlation was found between R value and SSD, and no obvious maximum was obtained for R value. The observed sensitivity of SSD to quality of data fitting is in good agreement with other studies by Christl and Kretzschmar [74] and Hwang and Lenhart [79]. Since the data fitting quality is insensitive to SSD while modeled pK_a values are not, fitting the potentiometric titration data by optimizing arbitrary SSD might impede the accuracy in determining pK_a values. In similar, Christl and Kretzschmar [74] noted that fitting the surface titration data would not be recommended for determining SSD.

Importantly, the results emphasize the need for consistency in SSD, pK_a values, and SCM type in any self-consistent SCM database. The framework presented here provides an approach to developing such a self-consistent database using the principles of FAIR community data.

4. Conclusions

In the present study, the community data-based surface complexation modeling framework was successfully developed and was utilized for iron oxide potentiometric titration systems to produce 'representative' protolysis constants that account for all potentiometric titration data collected from multiple literature sources. In addition, the influence of SCM type and effect of SSD on potentiometric titration modeling were examined.

Simulation results showed that the protolysis constants produced by the potentiometric titration data workflow can reproduce most of the experimental data with reasonable accuracy. The calculated protolysis constants showed a characteristic trend according to the type of iron oxide in the following order: magnetite < ferrihydrite < goethite < hematite. In particular, pK_a values of magnetite were significantly lower than that of the other three iron oxides, and the difference in iron oxidations states between magnetite and the other oxides is considered to be the most reasonable explanation for this feature. The order of protolysis constants of ferrihydrite, goethite, and hematite appear to be correlated with their thermodynamic stabilities.

SCM type had considerable effects on not only calculated pK_a values but also the quality of the model fit. Based on our ferrihydrite potentiometric titration case, pK_a values obtained using the NEM were significantly different from those obtained using the DDLM and CCM. In addition, typically, NEM showed markedly poor fit quality compared to the DDLM or CCM, and rarely reproduced the experimental data. SSD values used in the models also had a significant impact on the calculated pK_a values.

This study started with the aim of the construction of a self-consistent SCM database. Although enormous studies have shed light on the surface chemistry of oxide minerals (e.g., [17,25–28]), it was found that there was an impasse in the integration of the experimental data scattered in different studies and in obtaining a consensus among those studies. Since the different studies were based on divergent experimental conditions, it was required to develop a comprehensive SCM framework, which can reconcile the full community-wide data, in order to produce 'representative' reaction constants to be utilized in downstream sorption modeling. Until now, however, only a few limited studies have focused on this goal (e.g., [10,11,38]).

The work presented herein demonstrates a modeling approach to reconcile large amounts of potentiometric titration data for iron oxides. In addition, the present work shows that the application of community data-driven modeling can additionally identify erroneous datapoints. This feature can be investigated to increase the robustness and reliability of databases and/or surface complexation models. It is expected that the present study could help to bring consensus to the development of SCMs for iron oxide sorption systems by enabling the appropriate choice of protolysis constants for the quantification of mineral-adsorbate interactions. The results emphasize the need for consistency in SSD, pK_a values, and SCM type in any self-consistent SCM database. The framework presented here provides an approach to developing such a self-consistent database using the principles of FAIR community data. The framework also provides a path forward for developing self-consistent, comprehensive, and updateable surface complexation databases for nuclear waste disposal performance assessment and reactive transport modeling more broadly.

CRediT authorship contribution statement

Sol-Chan Han: Conceptualization, Methodology, Software, Formal analysis, Investigation, Writing – original draft, Writing – review & editing, Visualization, Funding acquisition. **Elliot Chang:** Conceptualization, Methodology, Software, Writing – original draft. **Susanne Zechel:** Methodology, Investigation. **Frank Bok:** Writing – original draft, Investigation. **Mavrik Zavarin:** Conceptualization, Methodology, Software, Formal analysis, Investigation, Writing – original draft, Writing – review & editing, Supervision, Funding acquisition.

Declaration of Competing Interest

The authors declare that they have no known competing financial interests or personal relationships that could have appeared to influence the work reported in this paper.

Data availability

Potentiometric titration data are available on the Environmental System Science Data Infrastructure for a Virtual Ecosystem (ESS-DIVE) page (https://ess-dive.lbl.gov/). The modeling workflows are available on the LLNL-Github page (https://github.com/LLNL/)..

Acknowledgements

This work was supported by Nuclear Global Fellowship Program through the Korea Nuclear International Cooperation Foundation (KONICOF) funded by the Ministry of Science and ICT, Republic of Korea. Additional support was provided by the Spent Fuel and Waste Science and Technology campaign of the Department of Energy's Nuclear Energy Program and the U.S. Department of Energy's Earth and Environmental Systems Sciences Division of the Office of Science Biological and Environmental Research program under contract SCW1053. This work is also funded by the Federal Company for Radioactive Waste Disposal (BGE) with the contract number EKFuE-21-03-js (SOREDA). This work was performed under the auspices of the U.S. Department of Energy by Lawrence Livermore National Laboratory under Contract DE-AC52-07NA27344.

Appendix A. Supplementary material

Supplementary data to this article can be found online at https://doi.org/10.1016/j.jcis.2023.06.054.

References

[1] K.M. Krupka, D.I. Kaplan, G. Whelan, R.J. Serne, S.V. Mattigod, Understanding variation in partition coefficient, K_d, values Volume II: Review of Geochamistry and Available K_d Values for Cadmium, Cesium, Chromium, Lead, Plutonium, Radon, Strontium, Thorium, Tritium(^{3}H), and Uranium, United States Environmental Protection Agency, Washington, DC, USA, 1999.

[2] K.M. Krupka, D.I. Kaplan, G. Whelan, R.J. Serne, S.V. Mattigod, Understanding variation in partition coefficient, K_d, values. Volume I: The K_d Model, Methods of Measurement, and Application of Chemical Reaction Codes, United States Environmental Protection Agency, Washington, DC, USA, 1999.

[3] P. Bertetti, R. Pabalan, D. Pickett, D. Turner, Radionuclide sorption technical assistance activities at the center for nuclear waste regulatory analyses, U.S. Nuclear Regulatory Commission, San Antonio, Texas, USA, 2011.
[4] J.A. Davis, D.E. Meece, M. Kohler, G.P. Curtis, Approaches to surface complexation modeling of Uranium(VI) adsorption on aquifer sediments, Geochim. Cosmochim. Acta 68 (18) (2004) 3621–3641.
[5] J.A. Davis, Surface Complexation Modeling of Uranium (VI) Adsorption on Natural Mineral Assemblages, U.S. Nuclear Regulatory Commission, Washington, DC, 2001.
[6] J.A. Davis, D.B. Kent, Chapter 5. surface complexation modeling in aqueous geochemistry, in: M.F. Hochella, A.F. White (Eds.), Mineral-Water Interface Geochemistry, MINERALOGICAL SOCIETY OF AMERICA, WASHINGTON, D.C., 1990, pp. 177–260.
[7] S. Goldberg, L.J. Criscenti, D.R. Turner, J.A. Davis, K.J. Cantrell, Adsorption-desorption processes in subsurface reactive transport modeling, Vadose Zone J. 6 (3) (2007) 407–435.
[8] B. Arora, J.A. Davis, N.F. Spycher, W. Dong, H.M. Wainwright, Comparison of electrostatic and non-electrostatic models for U(VI) sorption on aquifer sediments, Groundwater 56 (1) (2018) 73–86.
[9] W. Stumm, Chemistry of the Solid-Water Interface: Processes at the Mineral-Water and Particle-Water Interface in Natural Systems, John Wiley & Sons, New York, 1992.
[10] D.A. Dzombak, F.M.M. Morel, Surface complexation modeling: hydrous ferric oxide, John Wiley & Sons, 1990.
[11] A.K. Karamalidis, D.A. Dzombak, Surface Complexation Modeling: Gibbsite, John Wiley & Sons Inc, Hoboken, New Jersey, 2010.
[12] D.L. Parkhurst, C.A.J. Appelo, Description of input and examples for PHREEQC version 3—A computer program for speciation, batch-reaction, one-dimensional transport, and inverse geochemical calculations, US geological survey techniques and methods (2013) 497.
[13] C.I. Steefel, CrunchFlow: Software for Modeling Multicomponent Reactive Flow and Transport: USER'S MANUAL, Lawrence Berkeley National Laboratory, Berkeley, CA, 2009.
[14] J.A. Davis, R.O. James, J.O. Leckie, Surface ionization and complexation at the oxide/water interface: I. Computation of electrical double layer properties in simple electrolytes, J. Colloid Interface Sci. 63 (3) (1978) 480–499.
[15] T. Hiemstra, P. Venema, W.H. van Riemsdijk, Intrinsic proton affinity of reactive surface groups of metal (hydr)oxides: the bond valence principle, J. Colloid Interface Sci. 184 (2) (1996) 680–692.
[16] C. Tournassat, R.M. Tinnacher, S. Grangeon, J.A. Davis, Modeling uranium(VI) adsorption onto montmorillonite under varying carbonate concentrations: A surface complexation model accounting for the spillover effect on surface potential, Geochim. Cosmochim. Acta 220 (2018) 291–308.
[17] D.A. Sverjensky, N. Sahai, Theoretical prediction of single-site surface-protonation equilibrium constants for oxides and silicates in water, Geochim. Cosmochim. Acta 60 (20) (1996) 3773–3797.
[18] K.F. Hayes, G. Redden, W. Ela, J.O. Leckie, Surface complexation models: An evaluation of model parameter estimation using FITEQL and oxide mineral titration data, J. Colloid Interface Sci. 142 (2) (1991) 448–469.
[19] S. Goldberg, Surface Complexation Modeling, Reference Module in Earth Systems and Environmental Sciences, Elsevier, 2013.
[20] A.R. Vieira, Surface complexation modeling of Pb(II), Cd(II) and Se(IV) onto iron hydroxides in single and bisolute systems, Architectural, and Environmental Engineering, The University of Texas at Austin, Civil, 2006.
[21] G.S. Duffó, S.B. Farina, F.M. Schulz, Corrosion of steel drums containing cemented ion-exchange resins as intermediate level nuclear waste, J. Nucl. Mater. 438 (1) (2013) 116–125.
[22] H.I. Adegoke, F.A. Adekola, O.S. Fatoki, B.J. Ximba, Sorptive Interaction of Oxyanions with Iron Oxides: A Review, Pol. J. Environ. Stud. 22 (1) (2013) 7–24.
[23] C.V. Lazaratou, D.V. Vayenas, D. Papoulis, The role of clays, clay minerals and clay-based materials for nitrate removal from water systems: A review, Appl. Clay Sci. 185 (2020), 105377.
[24] R.M. Cornell, U. Schwertmann, The Iron Oxides: Structure, Properties, Reactions, Occurences and Uses, Second, Completely Revised and Extended, Edition ed., Wiley-VCH Verlag GmbH & Co. KGaA, Weinheim, Germany, 2003.
[25] C.-k.D. Hsi, D. Langmuir, Adsorption of uranyl onto ferric oxyhydroxides: Application of the surface complexation site-binding model, Geochim. Cosmochim. Acta 49 (9) (1985) 1931–1941.
[26] P. Trivedi, L. Axe, Ni and Zn Sorption to Amorphous versus Crystalline Iron Oxides: Macroscopic Studies, J. Colloid Interface Sci. 244 (2) (2001) 221–229.
[27] E.M. Moon, C.L. Peacock, Modelling Cu(II) adsorption to ferrihydrite and ferrihydrite–bacteria composites: Deviation from additive adsorption in the composite sorption system, Geochim. Cosmochim. Acta 104 (2013) 148–164.
[28] D.A. Sverjensky, Prediction of surface charge on oxides in salt solutions: Revisions for 1:1 (M^+L^-) electrolytes, Geochim. Cosmochim. Acta 69 (2) (2005) 225–257.
[29] S.M. Nomaan, S.N. Stokes, J. Han, L.E. Katz, Application of spectroscopic evidence to diffuse layer model (DLM) parameter estimation for cation adsorption onto ferrihydrite in single- and bi-solute systems, Chem. Geol. 573 (2021), 120199.
[30] V. Veselská, R. Fajgar, S. Číhalová, R.M. Bolanz, J. Göttlicher, R. Steininger, J. A. Siddique, M. Komárek, Chromate adsorption on selected soil minerals: Surface complexation modeling coupled with spectroscopic investigation, J. Hazard. Mater. 318 (2016) 433–442.
[31] D.S. Alessi, J.B. Fein, Cadmium adsorption to mixtures of soil components: Testing the component additivity approach, Chem. Geol. 270 (1–4) (2010) 186–195.
[32] C.J. Landry, C.M. Koretsky, T.J. Lund, M. Schaller, S. Das, Surface complexation modeling of Co(II) adsorption on mixtures of hydrous ferric oxide, quartz and kaolinite, Geochim. Cosmochim. Acta 73 (13) (2009) 3723–3737.
[33] T. Arnold, T. Zorn, G. Bernhard, H. Nitsche, Sorption of uranium(VI) onto phyllite, Chem. Geol. 151 (1–4) (1998) 129–141.
[34] B. Nowack, J. Lützenkirchen, P. Behra, L. Sigg, Modeling the Adsorption of Metal−EDTA Complexes onto Oxides, Environ Sci Technol 30 (7) (1996) 2397–2405.
[35] V. Brendler, A. Vahle, T. Arnold, G. Bernhard, T. Fanghänel, RES^{3}T-Rossendorf expert system for surface and sorption thermodynamics, J. Contam. Hydrol. 61 (1–4) (2003) 281–291.
[36] Helmholtz-Zentrum Dresden-Rossendorf, RES^{3}T-Rossendorf Expert System for Surface and Sorption Thermodynamics. www.hzdr.de/res3t.
[37] M.D. Wilkinson, M. Dumontier, I.J. Aalbersberg, G. Appleton, M. Axton, A. Baak, N. Blomberg, J.-W. Boiten, L.B. da Silva Santos, P.E. Bourne, J. Bouwman, A.J. Brookes, T. Clark, M. Crosas, I. Dillo, O. Dumon, S. Edmunds, C.T. Evelo, R. Finkers, A. Gonzalez-Beltran, A.J.G. Gray, P. Groth, C. Goble, J.S. Grethe, J. Heringa, P.A.C. 't Hoen, R. Hooft, T. Kuhn, R. Kok, J. Kok, S.J. Lusher, M.E. Martone, A. Mons, A.L. Packer, B. Persson, P. Rocca-Serra, M. Roos, R. van Schaik, S.-A. Sansone, E. Schultes, T. Sengstag, T. Slater, G. Strawn, M.A. Swertz, M. Thompson, J. van der Lei, E. van Mulligen, J. Velterop, A. Waagmeester, P. Wittenburg, K. Wolstencroft, J. Zhao, B. Mons, The FAIR Guiding Principles for scientific data management and stewardship, Scientific Data 3(1) (2016) 160018.
[38] M. Zavarin, E. Chang, H. Wainwright, N. Parham, R. Kaukuntla, J. Zouabe, A. Deinhart, V. Genetti, S. Shipman, F. Bok, V. Brendler, Community Data Mining Approach for Surface Complexation Database Development, Environ Sci Technol 56 (4) (2022) 2827–2838.
[39] J.A. Davis III, ADSORPTION OF TRACE METALS AND COMPLEXING LIGANDS AT THE OXIDE/WATER INTERFACE, Stanford University, 1978.
[40] S.B. Kanungo, D.M. Mahapatra, Interfacial properties of two hydrous iron oxides in KNO_3 solution, Colloids Surf. 42 (1) (1989) 173–189.
[41] H.F. Ghoneimy, T.N. Morcos, N.Z. Misak, Adsorption of Co^{2+} and Zn^{2+} ions on hydrous Fe(III), Sn(IV) and mixed Fe(III)/Sn(IV) oxides Part I, Characteristics of the hydrous oxides, apparent capacity and some equilibria measurements, Colloids and Surfaces A: Physicochemical and Engineering Aspects 122 (1–3) (1997) 13–26.
[42] J.A. Dyer, Advanced approaches for modeling trace metal sorption in aqueous systems, University of Delaware, 2003.
[43] A. Hofmann, W. van Beinum, J.C.L. Meeussen, R. Kretzschmar, Sorption kinetics of strontium in porous hydrous ferric oxide aggregates II. Comparison of experimental results and model predictions, J. Colloid Interface Sci. 283 (1) (2005) 29–40.
[44] T. Nagata, K. Fukushi, Y. Takahashi, Prediction of iodide adsorption on oxides by surface complexation modeling with spectroscopic confirmation, J. Colloid Interface Sci. 332 (2) (2009) 309–316.
[45] S. Pivovarov, Diffuse sorption modeling, J. Colloid Interface Sci. 332 (1) (2009) 54–59.
[46] J. Antelo, S. Fiol, C. Pérez, S. Mariño, F. Arce, D. Gondar, R. López, Analysis of phosphate adsorption onto ferrihydrite using the CD-MUSIC model, J. Colloid Interface Sci. 347 (1) (2010) 112–119.
[47] T. Nagata, K. Fukushi, Prediction of iodate adsorption and surface speciation on oxides by surface complexation modeling, Geochim. Cosmochim. Acta 74 (21) (2010) 6000–6013.
[48] L.S. Balistrieri, J.W. Murray, The surface chemistry of goethite (αFeOOH) in major ion seawater, Am. J. Sci. 281 (6) (1981) 788–806.
[49] N.J. Barrow, V.C. Cox, The effects of pH and chloride concentration on mercury sorption. I. By goethite, J. Soil Sci. 43 (2) (1992) 295–304.
[50] J. Bowden, S. Nagarajah, N. Barrow, A. Posner, J. Quirk, Describing the adsorption of phosphate, citrate and selenite on a variable-charge mineral surface, Soil Res. 18 (1) (1980) 49–60.
[51] T. Fujita, M. Tsukamoto, T. Ohe, S. Nakayama, Y. Sakamoto, Modeling of Neptunium(V) Sorption Behavior onto Iron-Containing Minerals, MRS Online Proc. Libr. 353 (1) (1994) 965–972.
[52] M. Gunnarsson, Z. Abbas, E. Ahlberg, S. Gobom, S. Nordholm, Corrected Debye-Hückel Analysis of Surface Complexation: II, A Theory of Surface Charging, Journal of Colloid and Interface Science 249 (1) (2002) 52–61.
[53] U. Hoins, L. Charlet, H. Sticher, Ligand effect on the adsorption of heavy metals: The sulfate — Cadmium — Goethite case, Water Air Soil Pollut. 68 (1) (1993) 241–255.
[54] K. Lackovic, M.J. Angove, J.D. Wells, B.B. Johnson, Modeling the adsorption of Cd(II) onto Muloorina illite and related clay minerals, J. Colloid Interface Sci. 257 (1) (2003) 31–40.
[55] D.O. Lumsdon, L.J. Evans, Surface Complexation Model Parameters for Goethite (α-FeOOH), J. Colloid Interface Sci. 164 (1) (1994) 119–125.
[56] T. Missana, M. García-Gutiérrez, C. Maffiotte,, Experimental and modeling study of the uranium (VI) sorption on goethite, J. Colloid Interface Sci. 260 (2) (2003) 291–301.
[57] B. Müller, L. Sigg, Adsorption of lead(II) on the goethite surface: Voltammetric evaluation of surface complexation parameters, J. Colloid Interface Sci. 148 (2) (1992) 517–532.
[58] A. Naveau, F. Monteil-Rivera, J. Dumonceau, S. Boudesocque, Sorption of europium on a goethite surface: influence of background electrolyte, J. Contam. Hydrol. 77 (1) (2005) 1–16.
[59] C.L. Peacock, D.M. Sherman, Copper(II) sorption onto goethite, hematite and lepidocrocite: a surface complexation model based on ab initio molecular

geometries and EXAFS spectroscopy1 1Associate editor: D. L. Sparks, Geochimica et Cosmochimica Acta 68(12) (2004) 2623-2637.
[60] R. Rahnemaie, T. Hiemstra, W.H. van Riemsdijk, A new surface structural approach to ion adsorption: Tracing the location of electrolyte ions, J. Colloid Interface Sci. 293 (2) (2006) 312–321.
[61] A.P. Robertson, J.O. Leckie, Cation Binding Predictions of Surface Complexation Models: Effects of pH, Ionic Strength, Cation Loading, Surface Complex, and Model Fit, J. Colloid Interface Sci. 188 (2) (1997) 444–472.
[62] A.P. Robertson, J.O. Leckie, Acid/Base, Copper Binding, and Cu^{2+}/H^{+} Exchange Properties of Goethite, an Experimental and Modeling Study, Environ Sci Technol 32 (17) (1998) 2519–2530.
[63] R.S. Rundberg, Y. Albinsson, K. Vannerberg, Sodium Adsorption onto Goethite as a Function of pH and Ionic Strength, Radiochimca Acta 66–67 (Supplement) (1994) 333–340.
[64] L. Sigg, Die Wechselwirkung von Anionen und schwachen Säuren mit α-FeOOH (Goethit) in wässriger Lösung, ETH Zürich, 1980.
[65] A. van Geen, A.P. Robertson, J.O. Leckie, Complexation of carbonate species at the goethite surface: Implications for adsorption of metal ions in natural waters, Geochim. Cosmochim. Acta 58 (9) (1994) 2073–2086.
[66] M. Villalobos, J.O. Leckie, Carbonate adsorption on goethite under closed and open CO_2 conditions, Geochim. Cosmochim. Acta 64 (22) (2000) 3787–3802.
[67] D.E. Yates, The structure of the oxide/aqueous electrolyte interface, University of Melbourne Australia, 1975.
[68] A. Breeuwsma, J. Lyklema, Interfacial electrochemistry of haematite (α-Fe_2O_3), Discuss. Faraday Soc. 52 (1971) 324–333.
[69] P. Hesleitner, D. Babic, N. Kallay, E. Matijevic, Adsorption at solid/solution interfaces. 3. Surface charge and potential of colloidal hematite, Langmuir 3 (5) (1987) 815–820.
[70] A.W.M. Gibb, L.K. Koopal, Electrochemistry of a model for patchwise heterogeneous surfaces: The rutile-hematite system, J. Colloid Interface Sci. 134 (1) (1990) 122–138.
[71] M. Čolić, D.W. Fuerstenau, N. Kallay, E. Matijević,, Lyotropic effect in surface charge, electrokinetics, and coagulation of a hematite dispersion, Colloids Surf. 59 (1991) 169–185.
[72] P. Hesleitner, N. Kallay, E. Matijevic, Adsorption at solid/liquid interfaces. 6. The effect of methanol and ethanol on the ionic equilibria at the hematite/water interface, Langmuir 7 (1) (1991) 178–184.
[73] S. Pivovarov, Acid-Base Properties and Heavy and Alkaline Earth Metal Adsorption on the Oxide-Solution Interface: Non-Electrostatic Model, J. Colloid Interface Sci. 206 (1) (1998) 122–130.
[74] I. Christl, R. Kretzschmar, Competitive sorption of copper and lead at the oxide-water interface: Implications for surface site density, Geochim. Cosmochim. Acta 63 (19/20) (1999) 2929–2938.
[75] M. Kohler, B.D. Honeyman, J.O. Leckie, Neptunium(V) Sorption on Hematite (α-Fe_2O_3) in Aqueous Suspension: The Effect of CO_2, 85(1-2) (1999) 33-48.
[76] N. Marmier, F. Fromage, Comparing Electrostatic and Nonelectrostatic Surface Complexation Modeling of the Sorption of Lanthanum on Hematite, J. Colloid Interface Sci. 212 (2) (1999) 252–263.
[77] R.J. Murphy, J.J. Lenhart, B.D. Honeyman, The sorption of thorium (IV) and uranium (VI) to hematite in the presence of natural organic matter, Colloids Surf A Physicochem Eng Asp 157 (1) (1999) 47–62.
[78] M. Gunnarsson, M. Rasmusson, S. Wall, E. Ahlberg, J. Ennis, Electroacoustic and Potentiometric Studies of the Hematite/Water Interface, J. Colloid Interface Sci. 240 (2) (2001) 448–458.
[79] Y.S. Hwang, J.J. Lenhart, The dependence of hematite site-occupancy standard state triple-layer model parameters on inner-layer capacitance, J. Colloid Interface Sci. 319 (1) (2008) 206–213.
[80] S.L. Estes, Y. Arai, U. Becker, S. Fernando, K. Yuan, R.C. Ewing, J. Zhang, T. Shibata, B.A. Powell, A self-consistent model describing the thermodynamics of Eu(III) adsorption onto hematite, Geochim. Cosmochim. Acta 122 (2013) 430–447.
[81] A.Y. Romanchuk, S.N. Kalmykov, Actinides sorption onto hematite: experimental data, surface complexation modeling and linear free energy relationship, Radiochim. Acta 102 (4) (2014) 303–310.
[82] A.E. Regazzoni, M.A. Blesa, A.J.G. Maroto, Interfacial properties of zirconium dioxide and magnetite in water, J. Colloid Interface Sci. 91 (2) (1983) 560–570.
[83] H. Tamura, E. Matijević, L. Meites, Adsorption of Co^{2+} ions on spherical magnetite particles, J. Colloid Interface Sci. 92 (2) (1983) 303–314.
[84] M.A. Blesa, N.M. Figliolia, A.J.G. Maroto, A.E. Regazzoni, The influence of temperature on the interface magnetite—aqueous electrolyte solution, J. Colloid Interface Sci. 101 (2) (1984) 410–418.
[85] H. Catalette, J. Dumonceau, P. Ollar, Sorption of cesium, barium and europium on magnetite, J. Contam. Hydrol. 35 (1–3) (1998) 151–159.
[86] N. Marmier, A. Delisée, F. Fromage, Surface Complexation Modeling of Yb(III), Ni (II), and Cs(I) Sorption on Magnetite, J. Colloid Interface Sci. 211 (1) (1999) 54–60.
[87] T. Missana, M. García-Gutiérrez, V. Fernńdez, Uranium (VI) sorption on colloidal magnetite under anoxic environment: experimental study and surface complexation modelling, Geochim. Cosmochim. Acta 67 (14) (2003) 2543–2550.
[88] C. Mayant, B. Grambow, A. Abdelouas, S. Ribet, S. Leclercq, Surface site density, silicic acid retention and transport properties of compacted magnetite powder, Physics and Chemistry of the Earth, Parts A/B/C 33 (14–16) (2008) 991–999.
[89] J. Doherty, PEST: Model-Independent Parameter Estimation, Watermark Numerical Computing, 2018.
[90] N.A. Heckert, J.J. Filliben, NIST Handbook 148: Dataplot Reference Manual, Volume 2: LET Subcommands and Library Functions, National Institute of Standards and Technology Handbook Series 2003.
[91] J.R. Taylor, An Introduction to error analysis, the study of uncertainties in physical measurements, Second Edition ed.,, University Science Books, Sausalito, California, 1997.
[92] M. Eibl, S. Virtanen, F. Pischel, F. Bok, S. Lönnrot, S. Shaw, N. Huittinen, A spectroscopic study of trivalent cation (Cm3+ and Eu3+) sorption on monoclinic zirconia (ZrO2), Appl. Surf. Sci. 487 (2019) 1316–1328.
[93] J. Neumann, H. Brinkmann, S. Britz, J. Lützenkirchen, F. Bok, M. Stockmann, V. Brendler, T. Stumpf, M. Schmidt, A comprehensive study of the sorption mechanism and thermodynamics of f-element sorption onto K-feldspar, J. Colloid Interface Sci. 591 (2021) 490–499.
[94] A.F. Gualtieri, P. Venturelli, In situ study of the goethite-hematite phase transformation by real time synchrotron powder diffraction, Am. Mineral. 84 (5–6) (1999) 895–904.
[95] F.M. Michel, L. Ehm, S.M. Antao, P.L. Lee, P.J. Chupas, G. Liu, D.R. Strongin, M.A. A. Schoonen, B.L. Phillips, J.B. Parise, The Structure of Ferrihydrite, a Nanocrystalline Material, Science 316 (5832) (2007) 1726–1729.
[96] N. Pailhé, A. Wattiaux, M. Gaudon, A. Demourgues, Correlation between structural features and vis–NIR spectra of α-Fe_2O_3 hematite and AFe_2O_4 spinel oxides (A=Mg, Zn), J. Solid State Chem. 181 (5) (2008) 1040–1047.
[97] K. Tsukimura, S. Sasaki, N. Kimizuka, Cation Distributions in Nickel Ferrites, Jpn. J. Appl. Phys. 36 (6R) (1997) 3609–3612.
[98] J.D.H. Donnay, D. Harker, A new law of crystal morphology extending the Law of Bravais, Am. Mineral. 22 (5) (1937) 446–467.
[99] C.F. Macrae, I. Sovago, S.J. Cottrell, P.T.A. Galek, P. McCabe, E. Pidcock, M. Platings, G.P. Shields, J.S. Stevens, M. Towler, P.A. Wood, Mercury 4.0: from visualization to analysis, design and prediction, J. Appl. Cryst. 53 (1) (2020) 226–235.
[100] R.M. Cornell, A.M. Posner, J.P. Quirk, Crystal morphology and the dissolution of goethite, J. Inorg. Nucl. Chem. 36 (9) (1974) 1937–1946.
[101] H. Guo, A.S. Barnard, Thermodynamic modelling of nanomorphologies of hematite and goethite, J. Mater. Chem. 21 (31) (2011) 11566–11577.
[102] A. Richter, V. Brendler, C. Nebelung, Blind prediction of Cu(II) sorption onto goethite: Current capabilities of diffuse double layer model, Geochim. Cosmochim. Acta 69 (11) (2005) 2725–2734.
[103] R.M. Cornell, R. Giovanoli, W. Schneider, Review of the hydrolysis of iron(III) and the crystallization of amorphous iron(III) hydroxide hydrate, J. Chem. Technol. Biotechnol. 46 (2) (1989) 115–134.
[104] J. Majzlan, A. Navrotsky, U. Schwertmann, Thermodynamics of iron oxides: Part III. Enthalpies of formation and stability of ferrihydrite (~$Fe(OH)_3$), schwertmannite (~$FeO(OH)_{3/4}(SO_4)_{1/8}$), and ε-$Fe_2O_3$, Geochim. Cosmochim. Acta 68 (5) (2004) 1049–1059.
[105] N. Pinney, J.D. Kubicki, D.S. Middlemiss, C.P. Grey, D. Morgan, Density Functional Theory Study of Ferrihydrite and Related Fe-Oxyhydroxides, Chem. Mater. 21 (24) (2009) 5727–5742.
[106] U. Schwertmann, J. Friedl, H. Stanjek, From Fe(III) Ions to Ferrihydrite and then to Hematite, J. Colloid Interface Sci. 209 (1) (1999) 215–223.
[107] M. Usman, K. Hanna, M. Abdelmoula, A. Zegeye, P. Faure, C. Ruby, Formation of green rust via mineralogical transformation of ferric oxides (ferrihydrite, goethite and hematite), Appl. Clay Sci. 64 (2012) 38–43.
[108] H. Wu, J.-J. Yin, W.G. Wamer, M. Zeng, Y.M. Lo, Reactive oxygen species-related activities of nano-iron metal and nano-iron oxides, J. Food Drug Anal. 22 (1) (2014) 86–94.
[109] J.M. Zachara, R.K. Kukkadapu, J.K. Fredrickson, Y.A. Gorby, S.C. Smith, Biomineralization of Poorly Crystalline Fe(III) Oxides by Dissimilatory Metal Reducing Bacteria (DMRB), Geomicrobiol J. 19 (2) (2002) 179–207.
[110] C.M. Flynn Jr., Hydrolysis of inorganic iron(III) salts, Chem. Rev. 84 (1) (1984) 31–41.
[111] B. Lu, H. Guo, P. Li, H. Liu, Y. Wei, D. Hou, Comparison study on transformation of iron oxyhydroxides: Based on theoretical and experimental data, J. Solid State Chem. 184 (8) (2011) 2139–2144.
[112] J. Lützenkirchen, The constant capacitance model and variable ionic strength: an evaluation of possible applications and applicability, J. Colloid Interface Sci. 217 (1) (1999) 8–18.